Remote Sensing of Environment 140 (2014) 766–778

Contents lists available at ScienceDirect

Remote Sensing of Environment

journal homepage: www.elsevier.com/locate/rse

An assessment of remote sensing algorithms for colored dissolved organic matter in complex freshwater environments

Weining Zhu [a,b], Qian Yu [c,*], Yong Q. Tian [a,b], Brian L. Becker [a,b], Tao Zheng [a,b], Hunter J. Carrick [a,d]

[a] Institute for Great Lakes Research, Central Michigan University, United States
[b] Department of Geography, Central Michigan University, United States
[c] Department of Geosciences, University of Massachusetts, Amherst, United States
[d] Department of Biology, Central Michigan University, United States

ARTICLE INFO

Article history:
Received 2 May 2013
Received in revised form 12 October 2013
Accepted 12 October 2013
Available online xxxx

Keywords:
CDOM
Algorithm
Freshwater environments
Saginaw River
Lake Huron

ABSTRACT

This study evaluated fifteen algorithms representing four major categories of retrieval algorithms for aquatic colored dissolved organic matter (CDOM): empirical, semi-analytical, optimization, and matrix inversion methods. The specific goal here was to evaluate (and understand) the strengths and limits of these algorithms in predicting CDOM dynamics along a gradient of varying water quality in a large, freshwater ecosystem. The data were collected in May and October of 2012 from the estuarine areas of the Kawkawlin and Saginaw Rivers, and Lake Huron. Algorithms were evaluated through comparisons to in-situ CDOM measurements, such that the analysis of these field measurements showed that CDOM levels in these areas displayed a range of CDOM absorption coefficients $a_{CDOM}(440)$ (0.1–8.5 m^{-1}). In general, the majority of the algorithms underestimated high CDOM waters ($a_{CDOM}(440)>2\,m^{-1}$) and overestimated low CDOM scenarios (<0.5 m^{-1}). Six algorithms that performed consistently better compared with the other models (overall RMSE of <0.45) in estimating in-situ CDOM levels were three empirical, two semi-analytical, and one MIM algorithms. Our analysis identified a set of parameters for the matrix inversion methods (MIM) that allow them to work effectively across a broad range of CDOM levels. Analysis of our results indicated that the most effective wavelengths/band locations for estimating CDOM could vary depending on the levels of spectral interference from high concentrations of particulate matter in the water column. In addition, our results suggest that including wavelengths > 600 nm in the algorithms improves CDOM estimation accuracy significantly, particularly for complex freshwater environments.

1. Introduction

Colored dissolved organic matter (CDOM), the photo-active component of dissolved organic carbon (DOC), is often viewed as a reliable tracer of DOC. Many study results reported good correlations between CDOM and DOC (Blough, Zafiriou, & Bonilla, 1993; Del Castillo, Coble, Morell, Lopez, & Corredor, 1999), but their real relationships are complicated by environmental factors and human related contaminations (Chen et al., 2004). Due to its chromophoric and optical properties, CDOM is capable of being estimated by remote sensing inversion algorithms. Early attempts of CDOM-related remote sensing were mainly focused on estimations from open sea environments where CDOM absorptivity is generally low and spatially homogeneous. Open sea CDOM is dominantly autochthonous through interactions with resident biological assemblages via formation and deposition (Nelson & Siegel, 2002). More recently, the estimation of CDOM in fresh, marine, or mixed water in both estuarine and coastal regions has been studied using a variety of techniques and applications (Miller, Del Castillo, & Mckee, 2005), aimed at assessing changes in salinity (Bowers & Brett, 2008) or the occurrence and distribution of red tides (Hu et al., 2005). To date, many CDOM estimation studies (Ammenberg, Flink, Lindell, Pierson, & Strombeck, 2002; Bracchini et al., 2006; Stedmon et al., 2006) have been directed towards inland relatively CDOM-rich freshwaters, where CDOM is greatly influenced by sources from land surface processes (i.e. allochthonous). Since suspended solids affect the optical properties of water containing CDOM, the optical estimations of CDOM in freshwaters are also affected by a variety of aquatic components, such as microbiological assemblages and suspended substances. In addition, CDOM absorptivity can be affected by environmental factors, such as hydrodynamics and anthropogenic activities (Hoge & Lyon, 2002). Accordingly, CDOM absorptivity (i.e. visible and near-IR) in inland freshwater environments can be quite high, with absorption coefficients as high as 20 m^{-1} (Brezonik, Menken, & Bauer, 2005).

As interest in estimating CDOM absorptivity in inland environments increases, accurate and robust algorithms will be needed. However, the

* Corresponding author at: Department of Geosciences, University of Massachusetts, 611 N Pleasant St., Amherst, MA 01003, United States. Tel.: +1 413 545 2095; fax: +1 413 545 1200.
E-mail address: qyu@geo.umass.edu (Q. Yu).

0034-4257/$ – see front matter © 2013 Elsevier Inc. All rights reserved.
http://dx.doi.org/10.1016/j.rse.2013.10.015

validity of previous and current CDOM estimation algorithms has not been well investigated.

Many CDOM estimation algorithms have been developed in the last three decades (IOCCG 2006), such as empirical (band ratios) (Mannino, Russ, & Hooker, 2008), semi-analytical/quasi-analytical (Lee, Carder, & Arnone, 2002; Lee et al., 2007; Zhu & Yu, 2013), matrix inversion methods (MIM) (Brando & Dekker, 2003; Hoge, Wright, Lyon, Swift, & Yungel, 1999; Wang, Boss, & Roesler, 2005), spectral matching (Liu & Miller, 2008), and artificial neural network (ANN) (Sandidge & Holyer, 1998; Tanaka & Oishi, 1998). Empirical approaches require less knowledge of the fundamental relationships between water's apparent and inherent optical properties, but require adequate data to parameterize the model. The primary limitation to empirical algorithms is that the derived relationship may only be valid for parameter specific locations. These algorithms are thus particularly sensitive to changes in the specific composition of water constituents when boundary conditions are changed (IOCCG, 2000).

Semi- or quasi-analytical algorithms incorporate both empirical parameters and bio-optical models (i.e. radiative transfer models). They describe the relationship between in-water constituents and water-leaving radiance or reflectance analytically or semi-analytically (IOCCG, 2000; Sathyendranath & Platt, 1997). The MIM algorithms also use some semi-analytical methodologies, but require knowledge about specific inherent optical properties (SIOPs) to be preset, such as the specific absorption coefficient of chlorophyll and the absorption slopes of CDOM and non-algal particles (Brando & Dekker, 2003). Again, because these parameters can be site specific, MIM approaches are generally not applicable across different environments without field measured SIOPs. Other algorithms, such as ANN and LUT, require multiple regions of interest to be painstakingly identified and delineated as input for forward spectral matching, making them difficult to apply to a large set of satellite images. While the above algorithms have been thoroughly developed and successfully applied to specific regional environments (i.e. open sea and coastal regions), their utility to make predictions across a range of varying water quality conditions, or within a single, complex freshwater ecosystem have not been sufficiently tested. Thus, it is necessary to evaluate the performance of current algorithms in complex freshwater environments, (i.e. inland river mouths) where CDOM absorptivity is often spatially and temporally quite diverse.

This study evaluated 15 CDOM estimation algorithms with samples collected within and near plume areas of the Kawkawlin and Saginaw Rivers, where each enters into Lake Huron. CDOM absorptivity is generally high, due to the terrestrial input from each watershed (i.e. forested and agricultural regions). We analyzed the relative strengths and weaknesses of these algorithms, as well as examined the influence that specific algorithm parameters had on their estimation performance (e.g. wavelength selection, CDOM absorption slopes).

2. Methods

2.1. Study sites

Sampling was conducted along a spatial gradient where two major tributaries (Kawkawlin and Saginaw Rivers) discharge into Saginaw Bay, Lake Huron; sites were selected to encompass the conditions within each river, the sediment plumes at their confluence into the bay, and conditions that reflected offshore waters of the inner bay (Fig. 1). The Saginaw River is the largest river flowing into the Saginaw Bay, with an overall length of 36 km and a watershed of 22,260 km^2. The headwaters of the Saginaw River are mainly forested, which represent approximately 30% of the overall watershed. The majority of the lower portions of the watershed are agricultural, which represent approximately 52% of the overall watershed. An additional 10% of the watershed is designated as wetland, which is largely found directly adjacent to the river channel.

The Kawkawlin River is a smaller river with an overall length of 28.2 km and a watershed of 647 km^2, whose mouth is less than a kilometer from that of the Saginaw River (Fig. 1). This watershed is dominated by deciduous forests (40.2%), with a significant amount of wetland habitat (7.9%) found adjacent to the channel. The rivers also differ in water clarity, with the Saginaw River typically clouded with a much heavier sediment load, while the Kawkawlin River generally discharges clearer but stained waters.

2.2. Field measurements

Field measurements were made on May 10, 2012 and October 18, 2012 at which time 10 and 18 samples were retrieved, respectively (Fig. 1). Whenever possible, the locations of sampling sites were kept constant between the two dates (GPS identified locations); this allowed for more meaningful seasonal inferences to be made between specific locations. Surface water samples were collected using a bucket, dispensed into amber bottles (polypropelyene 500 mL), and stored in a cooler kept at ambient water temperatures until further processed in the laboratory (within 6 h in Mount Pleasant, Michigan). Concurrent to the collection of water samples, above-surface spectra, including water leaving radiance L_t and sky radiance L_i, were measured via a HyperSAS (Hyperspectral Surface Acquisition System; Satlantic Inc.) spectroradiometer. A HyperOCR (Hyperspectral Ocean Color Radiometer) was also used to measure above-surface downwelling irradiance E_d. The HyperSAS and HyperOCR were deployed as outlined in their operation manuals, making sure to adjust the zenith and azimuth angles of the HyperSAS according to the solar position before the spectra were collected. The L_t sensor was pointed at the water surface at an angle of 40° from Nadir, and at an angle 90° from the sun's azimuth, the L_i sensor was at the identical azimuth angle with L_t and pointed to the sky at an angle of 40° from the Zenith, and the E_d sensor was mounted at the highest point of the boat. The HyperSAS is specially designed for use in an aquatic environment, in which L_t, L_i, and E_d are measured by three sensors simultaneously. Therefore spectra derived from this system are generally of higher quality/accuracy than those from other less robust instruments.

Once in the laboratory, water samples were filtered through GF/F glass microfiber membrane (0.70 μm) under low pressure (<5 atm). The filters were retained to measure chlorophyll-a pigment in support of a second research initiative. The filtrate was collected and CDOM absorbance $A(\lambda)$ within wavelength range 200–800 nm was measured by a Cray-60 spectroradiometer with a 1-cm cuvette and Milli-Q blank correction. CDOM absorption coefficients were determined by

$$a_{CDOM}(\lambda) = A(\lambda) \times \frac{\ln(10)}{Pathlength} = A(\lambda) \times 230.3. \quad (1)$$

The remote sensing reflectance (R_{rs}) required for nearly all of the CDOM estimation algorithms was calculated by

$$R_{rs} = \frac{L_t - \rho L_i}{E_d} \quad (2)$$

where $\rho = 0.028$ was set according to the operation manual of HyperSAS and Mobley (1999). A second filtrate sample was retained to determine DOC concentrations. DOC concentration was measured using a Shimadzu TOC-V analyzer with high temperature combustion (Vlahos, Chen, & Repeta, 2002). In this process, 50 μL injections of water samples were combusted at 800 °C and the sample DOC concentration was calculated from the resultant CO_2 measured with a non-dispersive infrared detector. Both response factors and blanks were compared with inter-comparison standards provided by J. Sharp (U. Delaware) and D. Hansell (U. Miami).

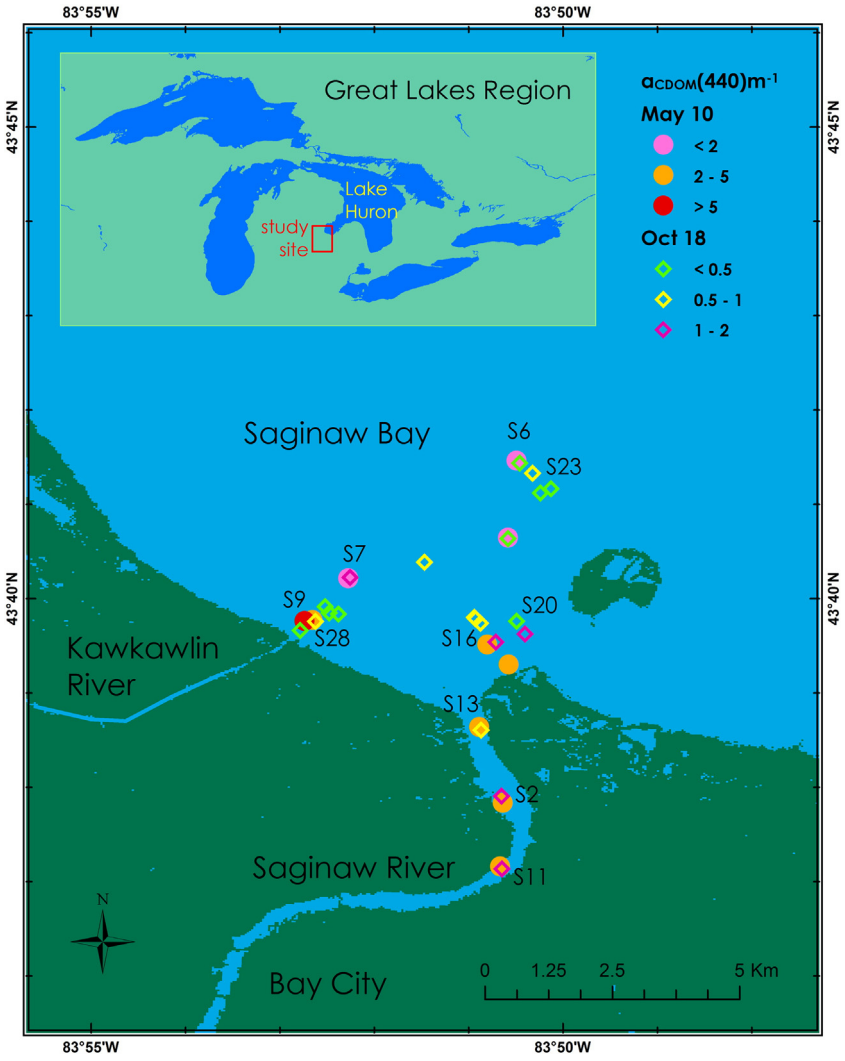

Fig. 1. Study site and sampling locations in the Saginaw River and Bay regions, Lake Huron in May and October, 2012.

We collected two samples at each sampling point during the first field trip to assess data uncertainty. Results from the 20 samples from the 10 sampling locations demonstrated that uncertainty was small (<5%). The small uncertainty achieved in the first cruise led to collecting only one sample for each of the 18 sampling points during our second cruise. Similarly, over 20 replicates of above-surface spectra at each sampling point also had small uncertainties (<3%). The median of the 20 spectra was used in the final analysis.

2.3. CDOM estimation algorithms

There are many existing algorithms available for estimating CDOM levels. These algorithms were developed with different focuses: algorithm categories, available water cases, specific remote sensing sensors, input wavelengths and parameters, and output CDOM proxies. We selected 15 algorithms representing four major categories of CDOM retrieval algorithms (Table 1): 8 empirical (EMP), 3 semi-analytical (SA), 1 optimization (OPT), and 3 matrix inversion methods (MIM). Algorithms with different versions, such as QAA-v4/v5 and Carder-1/2 (Carder, Chen, Lee, Hawes, & Kamykowski, 1999; IOCCG 2006; Lee, Lubac, Werdell, & Arnone, 2009; Lee et al., 2002) were treated as separate algorithms and evaluated independently. The algorithms proposed by Lyon, Brando, and Boss were all MIM, but varied from each other through the use of different wavelengths/bands and other parameters (Brando & Dekker, 2003; Brando, Dekker, Park, & Schroeder, 2012; Hoge & Lyon, 1996; Hoge, Wright, Lyon, Swift, & Yungel, 2001; Wang et al., 2005). The formulas of the 8 empirical algorithms (EMP) are listed in Appendix A. Note that there are additional existing empirical algorithms of detecting CDOM to that listed in Appendix A, such as those referenced in Matthews (2011).

The 15 algorithms range from those developed, calibrated, and validated within very specific environmental characteristics (e.g. Case 1, open ocean), to others that were developed to be applicable across a wide range of aquatic environments. The QAA, GSM, and Boss algorithms were developed using IOCCG (International Ocean Colour Coordinating Group) synthetic and in situ data, for open sea environments with low CDOM absorptivity (IOCCG 2006; Lee et al., 2002; Maritorena, Siegel, & Peterson, 2002). In contrast, the D'Sa and Del Castillo algorithms were developed with data collected from turbid water within the Mississippi River (Del Castillo & Miller, 2008; D'Sa & Miller, 2003). The algorithm introduced by Kutser (Kutser, Pierson, Kallio, Reinart, & Sobek, 2005; Kutser, Pierson, Tranvik, et al., 2005) was based on data collected from 34 lakes in Finland and Sweden, which likely makes it more applicable to inland waters in the Great Lakes of the United States.

Most algorithms require as input R_{rs} at several wavelengths across the visible electromagnetic spectrum (e.g., 410, 440, 490, 555, and 667 nm). These wavelength domains are within the band set of many ocean color satellite-based sensors (e.g. SeaWiFS, MODIS, and MERIS). A small

Table 1
CDOM retrieval algorithms considered in the study.

Algorithm name [a]	Type	Input R_{rs} (nm)	Output	Data sets/study sites	References
Brando	MIM	Multiple [b]	$a_{CDOM}(440)$	Fitzroy Estuary, Keppel Bay, etc.	(Brando & Dekker, 2003; Brando et al., 2012)
Lyon	MIM	412, 490, 555	$a_{dg}(440)$	IOCCG [c], U.S. Middle Atlantic Bight	(Hoge & Lyon, 1996; Hoge et al., 2001)
Boss	MIM	412, 443, 488, 510, 555	$a_{dg}(440)$	IOCCG, U.S. Middle Atlantic Bight	(IOCCG 2006; Wang et al., 2005)
GSM	OPT	412, 443, 490, 510, 555	$a_{dg}(440)$	IOCCG, a quasi-real dataset	(Maritorena et al., 2002)
QAA-v4	SA	410, 440, 490, 555, 640	$a_{dg}(443)$	IOCCG, Baja California	(Lee et al., 2002, 2007)
QAA-v5	SA	410, 440, 490, 555, 667	a_{dg} (443)	IOCCG, NOMAD [d]	(Lee et al., 2009)
QAA-CDOM	SA	440, 490, 555, 640	a_{CDOM} (440)	IOCCG, NOMAD, Hudson, Mississippi, Neponset, etc.	(Zhu et al., 2011; Zhu & Yu, 2013)
Carder-1	EMP	412, 443, 551	a_{dg} (443)	W Florida Shelf, Bayboro Harbor	(Carder et al., 1999; IOCCG 2006)
Carder-2	EMP	443, 488, 551, 667	a_{dg} (443)	W Florida Shelf, Bayboro Harbor	(Carder et al., 1999; IOCCG 2006)
Mannino	EMP	490, 555	$a_{CDOM}(443)$	U.S. Middle Atlantic Bight	(Mannino et al., 2008)
D'sa	EMP	443, 510	$a_{CDOM}(412)$	Mississippi River	(D'Sa & Miller, 2003)
Griffin	EMP	450–520, 520–600, 630–690 [e]	$a_{CDOM}(400)$	Kolyma River, East Siberia	(Griffin et al., 2011)
Kutser	EMP	525–605, 630–690 [f]	$a_{CDOM}(420)$	34 lakes in Finland and Sweden	(Kutser, Pierson, Tranvik, et al., 2005)
Castillo	EMP	510, 670	$a_{CDOM}(412)$	Mississippi River	(Del Castillo & Miller, 2008)
Ficek	EMP	570, 655	$a_{CDOM}(440)$	Pomeranian lakes and the Baltic	(Ficek et al., 2011)

[a] We use the names of their primary developers to refer to algorithms, except QAA and QAA-CDOM.
[b] The bands required are flexible (at least 3 bands). Here we used 410, 440, 490, 510, 555, 640, and 667.
[c] Synthetic and in situ data provided by IOCCG (International Ocean Colour Coordinating Group).
[d] The NASA Bio-optical Marine Algorithm Data set.
[e] Atmospherically corrected radiance reflection R at Bands 3, 4 and 5 of Landsat TM and ETM+.
[f] Atmospherically corrected radiance reflection R at Bands 2 and 3 of EO-1 ALI.

number of algorithms (e.g. Kutser and Griffin) require radiance reflectance R across broader wavelength domains, such as 525–605 nm and 630–690 nm provided by Landsat TM, ETM+ and EO-1 ALI. Although some remote sensing scientists have contended that land-oriented sensors are not suitable for aquatic research, there have been several successful efforts of using ALI and TM/ETM+ for CDOM estimation (Griffin, Frey, Rogan, & Holmes, 2011; Kutser, Pierson, Tranvik, et al., 2005).

Ultimately, most of the tested algorithms generated CDOM absorption coefficients $a_{CDOM}(\lambda)$ at 440 or 443 nm, which are widely accepted as the proxy of CDOM content. In this study we use $a_{CDOM}(440)$ to describe the amount of CDOM in the water and also assume that $a_{CDOM}(443) \approx a_{CDOM}(440)$. For a few algorithms that had an output $a_{CDOM}(\lambda)$ at 400, 412 or 420 nm, we converted them to $a_{CDOM}(440)$ using the below equation:

$$a_{CDOM}(440) = a_{CDOM}(440)e^{S(\lambda-440)} \tag{3}$$

where $\lambda = 400$, 412 or 420, and S is the slope describing the exponential decay of CDOM absorption coefficients with an increase in wavelength. Generally, S varies from -0.01 to -0.03 (Blough & Vecchio, 2001). For this investigation, S was set at -0.015 in order to reduce bias as recommended in previous studies (Blough & Vecchio, 2001). Another limitation of several algorithms (i.e. QAA-v4/v5) is that they produced a hybrid absorption coefficient a_{dg} rather than the a_{CDOM}. The hybrid coefficient a_{dg} is the absorption coefficient of detritus a_d and CDOM a_{CDOM} combined. The effect of using such a hybrid coefficient is viewed as negligible when applied to clear seawater where detrital materials are usually present at very low concentrations. However, it is likely that a significant error was introduced when using such a hybrid coefficient for turbid inland waters, where detrital effects cannot be ignored (Zhu, Yu, Tian, Chen, & Gardner, 2011).

Table 2
Measured optical and biochemical properties of 10 selected samples.

Sample #	Date	Site	$a_{CDOM}(440)$ (m^{-1})	Slope	DOC (mg/L)	Chl-a (mg/m^3)
S2	May	Saginaw	3.45	0.0165	10.24	11.35
S6	May	Huron	0.73	0.0165	5.42	3.85
S7	May	Kawkawlin	1.55	0.0172	6.97	3.64
S9	May	Kawkawlin	8.46	0.0158	17.86	10.12
S11	Oct.	Saginaw	2.06	0.0142	5.90	31.64
S13	Oct.	Saginaw	0.99	0.0191	5.96	10.47
S16	Oct.	Saginaw	1.75	0.0132	5.59	33.32
S20	Oct.	Saginaw	0.53	0.0116	3.51	8.26
S23	Oct.	Huron	0.11	0.0253	3.33	7.70
S28	Oct.	Kawkawlin	0.18	0.0204	3.44	15.23

Note: The slopes were determined by non-linear fitting through 300–750 nm.

2.4. Assessment statistics

We evaluated the performance of algorithms based upon four statistical metrics: *bias*, *AME* (Absolute Mean Error), *RMSE* (Root Mean Squared Error, in log space), and R^2 (regression, Type II) (IOCCG 2006).

Bias was defined as:

$$bias = \frac{\sum_{i=1}^{n}\left(x_i^{estimated} - x_i^{measured}\right)}{n} \tag{4}$$

AME was defined as:

$$AME = \frac{\sum_{i=1}^{n}\left(\left|\frac{x_i^{estimated} - x_i^{measured}}{x_i^{measured}}\right|\right)}{n} \tag{5}$$

RMSE was defined as:

$$RMSE = \sqrt{\frac{\sum_{i=1}^{n}\left[\log\left(x_i^{estimated}\right) - \log\left(x_i^{measured}\right)\right]^2}{n-2}} \tag{6}$$

where:

$$Error_{log} = \log\left(x^{estimated}\right) - \log\left(x^{measured}\right). \tag{7}$$

Log-based error is generally used for variables (e.g., CDOM and other ocean color components) with logarithmic distributions (IOCCG 2006).

3. Results and discussions

3.1. Measured optical and biological properties

Our results showed that spatial distributions and seasonal differences of the biological, chemical and optical water properties were quite large along the river-bay gradient sampled. Table 2 shows the measured DOC and chlorophyll-a concentrations, CDOM absorption coefficients and spectral slopes of 10 selected samples. These results demonstrated a

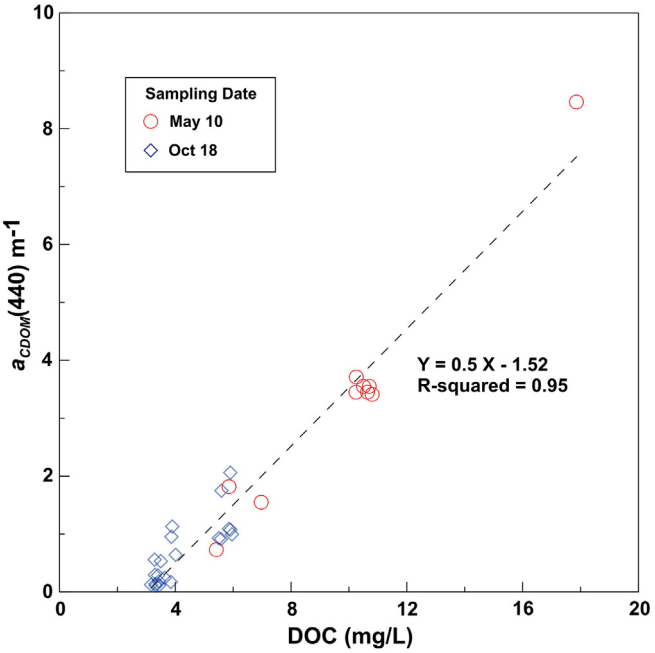

Fig. 2. Correlations between CDOM absorption coefficients and DOC concentrations.

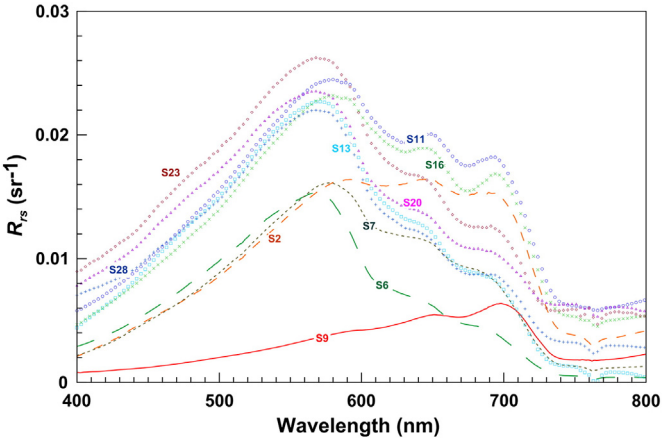

Fig. 3. Measured above-surface spectra (*Rrs*) of 10 selected samples. Lines are samples (S2, S6, S7, and S9) from May 10 and symbol dots are samples (S11, S13, S16, S20, S23, and S28) from October 18.

strong correlation ($R^2 = 0.93$) between CDOM and DOC (Fig. 2). The range of sampled CDOM levels $a_{CDOM}(440)$ was wide (0.11 m^{-1} to 8.46 m^{-1}) with a mean value of 1.69 m^{-1}, and the range of chl-a is 1.62–43.68 mg/m^3 with mean value of 14.77 mg/m^3. Our results also showed that the modeled CDOM and DOC variations were strongly related to terrestrial vegetation sources. For example, the May 10 samples indicated that $a_{CDOM}(440)$ was 8.5 m^{-1} and DOC was 14 mg/L within the Kawkawlin River plume area. These values were higher than the similar May 10 values measured for the Saginaw River; CDOM (~3.5 m^{-1}) and DOC (10.5 mg/L). The October sample values displayed similar trends (Fig. 2), for the Kawkawlin River plume area values (CDOM 2.07 m^{-1} and DOC 6.2 mg/L) were also higher than those of the Saginaw River (CDOM 1.03 m^{-1} and DOC 4 mg/L). These consistently higher CDOM and DOC levels were attributed to the dissimilarity of the two watersheds (Note that many samples near the river plume may be mixtures of more than one end-member). Recall that the Kawkawlin River watershed is predominantly forested while the Saginaw River watershed is predominantly agricultural land.

Seasonal CDOM and DOC differences in the Saginaw River watershed were indicated by the significant difference between the May and October sample dates. CDOM sampled in early May was marked higher (0.73–8.46 m^{-1}, mean 3.39 m^{-1}) due to snow melt that drives DOC and CDOM from the soil-based carbon pool to rivers and lakes (Huang & Chen, 2009). Spring time soil DOC and CDOM levels are often elevated because biological decay and chemical transformations of the accumulated autumn leaf-fall that occurred under the thick winter snow cover. As the potential sources of CDOM, organic litter and debris at soil surface are lower in early fall before fallen deciduous leaves accumulate. In addition, photo-oxidation and bacterial activities may also consume CDOM and hence make its levels lowest during the summer and early fall. Accordingly, the highest CDOM (8.46 m^{-1}) and DOC (17.9 mg/L) levels were recorded in the Kawkawlin River plume area on May 10, while the lowest CDOM and DOC (0.1 m^{-1} and 3.3 mg/L) levels were sampled on Oct. 18. These resulting CDOM level changes could be caused by some seasonal climate events such as rainfall or other ecological effects such as defoliation and algal bloom. More time-series samples are required in order to analyze environmental and seasonal scenarios.

The variability of above-surface spectra (R_{rs}) corresponded to variations of water CDOM levels well (Fig. 3). The magnitudes of R_{rs} were generally higher on Oct. 18 (S_{11}–S_{28}) where CDOM levels were lower than those on May 10 (S_2 and S_9), particularly within 400–550 nm. The measured R_{rs} over low-CDOM waters collected on Oct. 18 (S_{11}–S_{28}) fell in a similar range to that collected in May 10 (S_6 and S_7). However, the R_{rs} curve displayed markedly different shapes for low-CDOM vs. high-CDOM waters (S_2 and S_9). One noticeable difference is that the spectra at wavelengths >570 nm of low-CDOM samples (all but S_2 and S_9) have a decreasing trend. In contrast, spectra of the high-CDOM samples (S_2 in the Saginaw River and S_9 in the Kawkawlin River) either remained flat or increased between 570 nm and <700 nm. All of the spectra displayed a decreasing trend after 700 nm. In addition, the spectral features around 665 nm may also be affected by high chl-a concentration. These diagnostic spectral features highlight how essential it is to collect high quality in-situ spectra in order to investigate the remote sensing of CDOM in freshwater environments.

3.2. Evaluation of algorithm performance

3.2.1. Overall performance

Overall, the performance of the tested CDOM algorithms varied greatly in the complex freshwaters of the study site. General evaluation statistics for all algorithms were: RMSE = 0.57, AME = 90%, Bias = −0.71, and $R^2 = 0.58$ (Table 3 and Fig. 4). These statistics illustrated that the CDOM estimation errors are generally much larger than those generated from scenarios of open-sea waters (RMSE 0.2 – 0.3, IOCCG 2006). SA algorithms consistently outperform the others, displaying lower error (RMSE 0.32) than the empirical (RMSE 0.65) and MIM algorithms. A common characteristic of these algorithms is the overestimation for low-CDOM waters and underestimation for high-CDOM waters (Table 3 and Fig. 5). Three algorithms (QAA-CDOM, QAA and Carder-2) consistently outperformed the others, with an overall RMSE <0.35. A second tier of algorithms (i.e. Brando, Ficek, Kutser and Del Castillo) resulted in acceptable accuracies, with RMSE values ranging from 0.35 to 0.5. The CDOM estimations from the remaining eight algorithms displayed relatively large errors (RMSE >0.5).

In addition, several algorithms generated invalid CDOM estimates (i.e. negative $a_{CDOM}(440)$ values) when existing model parameters were used. For example, the GSM algorithm returned positive $a_{CDOM}(440)$ values for only 2 out of 28 samples. Therefore, this algorithm was excluded from further comparison and discussion (Table 4).

Across all model/algorithm types, six algorithms (Brando-2, QAA-v5, Carder-2, QAA-CDOM, Kutser, and Ficek) produced good estimations (RMSE <0.45) relative to the others. A common weakness of these six algorithms is overestimation for low-CDOM cases ($Error_{log} > 0.4$),

Table 3
Algorithm evaluations for different samples groups (CDOM levels, dates, and locations). The three lowest RMSE values within each subcategory are shown underlined. The *n* indicates the number of samples with each sub-category.

Algorithms	Bias	AME	RMSE	R^2	RMSE							
	All samples				$a_{CDOM}(440)$			Date		Location		
					<0.75	0.9–2.1	>3.4	May	Oct.	Kaw.	Sag.	Hur.
	$n = 28$				$n = 10$	$n = 11$	$n = 7$	$n = 10$	$n = 18$	$n = 7$	$n = 13$	$n = 8$
QAA-CDOM	0.12	0.45	0.29	0.82	0.29	0.37	0.19	0.2	0.34	0.38	0.25	0.37
QAA-v4	−0.81	0.57	0.35	0.5	0.32	0.37	0.46	0.38	0.35	0.51	0.3	0.38
QAA-v5	−0.58	0.52	0.31	0.45	0.34	0.3	0.39	0.32	0.32	0.49	0.23	0.36
Carder-1	−1.64	0.9	1.43	0.01	0.89	1.54	2.25	1.97	1.17	1.59	1.61	1.34
Carder-2	1.32	1.02	0.35	0.86	0.5	0.24	0.35	0.32	0.38	0.5	0.26	0.47
Mannino	−1.51	0.72	0.89	0.45	0.4	0.93	1.5	1.29	0.67	1.03	1.01	0.76
D'Sa	−1.43	0.7	0.75	0.31	0.34	0.77	1.29	1.08	0.57	0.91	0.85	0.59
Ficek	0.43	1.67	0.45	0.89	0.75	0.28	0.05	0.16	0.56	0.67	0.31	0.61
Del Castillo	−0.97	0.86	0.46	0.54	0.5	0.36	0.68	0.64	0.37	0.63	0.39	0.57
Kutser-n	−0.16	1.59	0.45	0.84	0.74	0.28	0.18	0.31	0.53	0.68	0.25	0.66
Kutser-w	0.44	1.9	0.48	0.87	0.8	0.31	0.06	0.24	0.59	0.73	0.31	0.66
Griffin-n	−1.28	0.84	0.61	0.35	0.38	0.56	1.08	0.91	0.44	0.79	0.65	0.54
Griffin-w	−1.25	0.87	0.6	0.21	0.39	0.52	1.08	0.9	0.43	0.8	0.64	0.53
Lyon	−1.31	0.65	0.61	0.34	0.32	0.65	1	0.82	0.51	0.79	0.66	0.49
Brando-1	−0.72	0.76	0.36	0.87	0.45	0.26	0.48	0.41	0.35	0.46	0.33	0.43
Brando-2	−0.77	0.76	0.37	0.87	0.44	0.27	0.51	0.44	0.35	0.47	0.35	0.43
Boss-1	−1.26	0.69	0.7	0.64	0.31	0.74	1.43	1.16	0.53	0.7	0.86	0.55
Boss-2	−1.38	0.7	0.76	0.61	0.33	0.8	1.4	1.15	0.57	0.86	0.89	0.66
Mean	−0.71	0.9	0.57	0.58	0.47	0.53	0.8	0.71	0.5	0.72	0.56	0.58

Note:
a. The first number 1 or 2 in Brando and Boss denotes the values of g_0 and g_1 that are set for the Case 1 or the Case 2 water. The criterion $C = 2$ used in the Brando and $C = 0.5$ used in the Boss.
b. The letter 'n' or 'w' in Griffin and Kutser denote using 'narrow' or 'wide' bands.

especially for those where $a_{CDOM}(440) < 0.2\ m^{-1}$ (Fig. 6). These poor estimations for low CDOM cases indicate that the 15 algorithms are insufficient for the weak optical signals generated via CDOM-poor complex freshwater estuarine environments such as our study site. The QAA-CDOM algorithm outperformed (overall RMSE 0.29) all other algorithms for extreme high DOC and CDOM scenarios, such as the highly varied and stained waters of the Kawkawlin River (RMSE 0.19).

3.2.2. Empirical algorithms

Three of the best performing six algorithms were empirical algorithms: Carder-2, Kutser, and Ficek. The Ficek and Kutser algorithms were developed specifically for the application to inland freshwater and did indeed outperform those developed specifically to open-sea, low CDOM environments (e.g., Carder-1 and Mannino). The algorithm of Kutser et al was developed based on field data collected from 34 Scandinavian inland freshwater lakes (Kutser, Pierson, Kallio, et al., 2005; Kutser, Pierson, Tranvik, et al., 2005), and the algorithm of Ficek et al was developed from 15 freshwater Pomeranian lakes (Ficek, Zapadka, & Dera, 2011). Both algorithms of Ficek et al and Kutser et al performed much better when applied to high-CDOM waters where $a_{CDOM}(440) > 3.4\ m^{-1}$ (RMSE: Ficek 0.05 and Kutser 0.06) than low-CDOM waters where $a_{CDOM}(440) < 0.75\ m^{-1}$ (RMSE: Ficek 0.75 and Kutser 0.8). Our resulting R^2 values (Kutser 0.83, Ficek 0.89) were also consistent to that in Kutser's and Ficek's original reports (Kutser 0.84, Ficek 0.85). In contrast, the Carder-2 algorithm was derived from a relative large and diverse saltwater dataset ($n = 319$) along the West Florida Coast and in Bayboro Harbor (IOCCG, 2006). Accordingly,

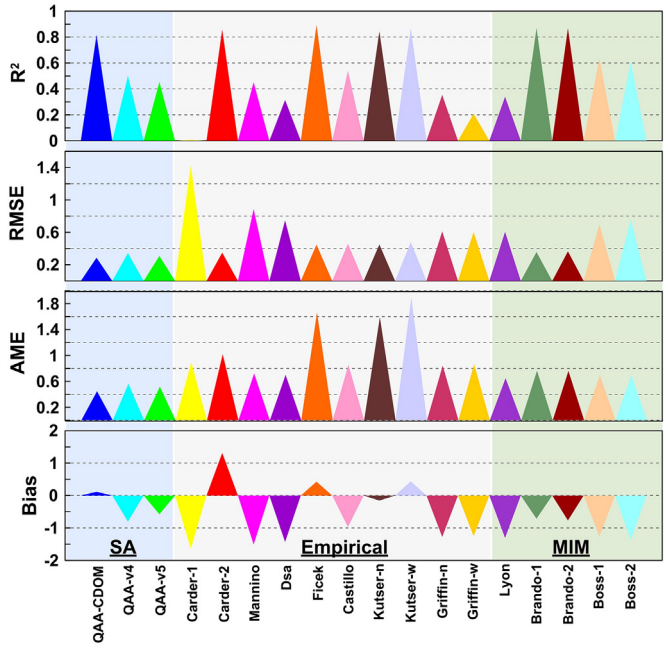

Fig. 4. Assessment (R^2, RMSE, AME, and Bias) of 15 CDOM retrieval algorithms for all samples.

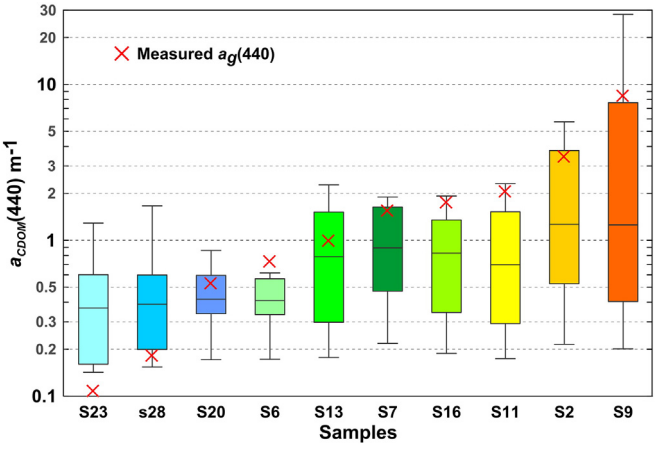

Fig. 5. Comparison between measured and derived $a_{CDOM}(440)$ for 10 typical samples, in Box–Whisker plot showing the derived 25%, 75%, median (50%), minimum, and maximum from all algorithms.

Table 4
The measured vs. estimated CDOM absorption coefficients $a_{CDOM}(440)$ for 10 typical samples. The bold values indicate their errors <25% and the underlined values are the best three results or algorithms. Note: Carder-1's results are excluded from statistics.

Sample #	S23	S28	S20	S6	S13	S7	S16	S11	S2	S9
Measured	0.11	0.18	0.53	0.73	0.99	1.55	1.75	2.06	3.45	8.46
QAA-CDOM	0.16	**0.20**	**0.42**	**0.62**	**0.78**	**1.90**	0.91	0.70	**3.86**	**8.04**
QAA-v4	0.25	0.29	**0.52**	**0.55**	0.60	**1.25**	0.70	0.61	1.69	1.25
QAA-v5	0.27	0.32	**0.58**	**0.57**	**0.79**	**1.64**	0.86	0.83	2.30	1.34
Carder-1	0.05	0.05	0.05	0.05	0.05	0.05	0.05	0.05	0.05	0.04
Carder-2	0.60	0.60	**0.58**	**0.55**	1.52	**1.67**	**1.35**	**1.60**	5.75	28.1
Mannino	0.16	**0.15**	0.17	0.19	0.18	0.22	0.19	0.17	0.21	0.20
D'Sa	0.16	**0.18**	0.25	0.33	0.24	0.37	0.25	0.24	0.32	0.28
Ficek	1.15	1.21	0.85	0.53	2.21	**1.63**	**1.92**	**2.31**	**3.76**	**7.62**
Del Castillo	0.55	0.55	**0.41**	0.17	**0.87**	0.84	0.83	0.88	1.07	1.19
Kutser-n	1.13	1.37	0.68	0.32	1.72	0.89	**1.41**	1.52	**2.62**	5.78
Kutser-w	1.29	1.66	0.86	0.33	2.27	**1.36**	**1.91**	**2.00**	**4.00**	**7.84**
Griffin-n	0.37	0.39	0.36	0.37	0.41	0.47	0.41	0.41	0.53	0.40
Griffin-w	0.39	0.41	**0.40**	0.42	0.43	0.50	0.44	0.44	0.54	0.38
Lyon	**0.14**	**0.18**	0.34	0.41	0.29	0.63	0.34	0.29	0.58	0.39
Brando-1	0.45	0.51	**0.60**	**0.57**	**1.03**	**1.25**	1.06	1.02	1.33	3.70
Brando-2	0.43	0.49	**0.58**	**0.57**	**0.94**	**1.20**	0.99	0.93	1.26	3.58
Boss-1	0.18	**0.20**	0.23	0.38	0.30	0.31	0.30	0.29	0.25	0.70
Boss-2	0.15	**0.18**	0.22	0.35	0.27	0.30	0.27	0.25	0.24	0.65
Min	0.14	0.15	0.17	0.17	0.18	0.22	0.19	0.17	0.21	0.20
Mean	0.46	0.52	0.47	0.43	0.87	0.97	0.83	0.85	1.78	4.20
Max	1.29	1.66	0.86	0.62	2.27	1.90	1.92	2.31	5.75	28.1
Bias	0.35	0.34	−0.06	−0.30	−0.12	−0.58	−0.92	−1.21	−1.67	−4.26
AME	3.19	1.92	0.33	0.42	0.57	0.43	0.55	0.60	0.60	0.78

Carder-2 performed better for medium to low-CDOM waters (Table 3 and Fig. 6a), wherein conditions emulate those of open ocean environments. The results of Carder et al (IOCCG, 2006) also show that using Carder-2 can reduce the RMSE error by 40% when compared to Carder-1. These results indicate that empirical models established with large data sets from broad environmental conditions can indeed work well within complex freshwater environments where $a_{CDOM}(440) < 1\ m^{-1}$.

We would like to emphasize that in addition to the sample size and geographical/environmental characteristics of the data used for developing empirical CDOM algorithms, there are many other factors, such as band selections, function forms and coefficients, which may significantly change the algorithm performance. For example, Carder-1 based the same data used by Carder-2, D'Sa and Griffin algorithms were both based on inland waters, but their performances were relatively poor. Therefore empirical algorithms may not necessarily work well in similar environmental/data context, while they might be good for different environments if their bands, functions, and parameters were accurately determined. In this study we mainly focus on band issues and will discuss them in Section 3.2.5.

3.2.3. Semi-analytical algorithms

The two best performing algorithms out of the 15 tested were the QAA-CDOM and QAA-v5 algorithms. QAA-CDOM was the most resilient, and able to handle extreme CDOM levels better than QAA v5, although it is often underestimated when applied to medium-CDOM waters (Table 3 and Fig. 6a). The unique improvement of QAA-CDOM over QAA v5 is that (1) it separated a_{dg} into a_{CDOM} (CDOM absorption coefficient) and a_d (absorption coefficient of non-algal particles) and (2) the equations/parameters of QAA-CDOM have been optimized from both a large synthetic and in situ data set that emulate broad environment conditions. Furthermore, QAA-CDOM's applicability to diverse water types has been widely validated (Zhu, 2011; Zhu, Tian, Yu, & Becker, 2013; Zhu & Yu, 2013; Zhu, Yu, & Tian, 2013; Zhu et al., 2011). Our results confirmed the advantages of separately quantifying a_{CDOM} and a_d and parameter optimization for low and high-CDOM waters, particularly for those turbid inland waters. For low-CDOM inland waters, detrital effects on absorptivity are often quite significant. Thus algorithms that do not separate absorption coefficients into CDOM and detrital components typically overestimated measured CDOM. For high-CDOM waters, QAA-v5 largely underestimated the measured CDOM. The overestimation is due to the fact that its empirical steps (for example, the step 2 to calculate the total absorption coefficient $a(555)$) and parameterization were derived from open-sea water (Zhu & Yu, 2013), and hence it is not well suited for relatively high-CDOM inland waters. QAA-CDOM is indeed optimized for a broader range of CDOM absorptivity, and represents a significant improvement over the QAA-v5 algorithm for high-CDOM waters. Compared to the previous version QAA-v4, QAA-v5 improved estimations slightly when our in-situ remote sensing data was used. Contrarily, QAA-v4 could perform better than the QAA-v5 when using a NOMAD data set (Lee et al., 2009).

3.2.4. Effects of parameterization on MIM algorithms

MIM algorithms were originally developed by Hoge and Lyon (1996). They retrieve many IOPs, such as a_{ph}, a_{dg}, and b_{bp} (particulate backscattering), by solving a group of equations. Each equation makes a simple connection between R_{rs} and IOPs at a given wavelength, namely, $R_{rs}(\lambda) = f(a(\lambda), b(\lambda))$, where $a(\lambda)$ and $b(\lambda)$ can be further expressed by the sum of each aquatic optical component, e.g., $a(\lambda) = a_w(\lambda) + a_{ph}(\lambda) + a_d(\lambda) + a_{CDOM}(\lambda)$. In order to solve the equation group, MIM algorithms also use some new formulae, such as Eq. (3), to link IOPs at different wavelengths. If the equation number is greater than the IOPs number, then the unknown IOPs can be derived from the best optimized solutions, which minimize the difference between the measured R_{rs} and calculated R_{rs} by equations.

As with many algorithms, changing operation parameters can fundamentally change estimation performance. It is imperative to have sufficient in situ measurements so that MIM algorithm parameters can be effectively calibrated in order to enhance overall estimation performance. The Brando-2 algorithm is representative of the MIM algorithms. It returned its most accurate results for medium CDOM waters ranging from 0.5 to 2 m^{-1}. However, it both overestimated for low-CDOM water and underestimated for high-CDOM waters. Upon comparison to the empirical and SA algorithms, the MIM algorithms required a higher degree of local observations (in situ measurements)

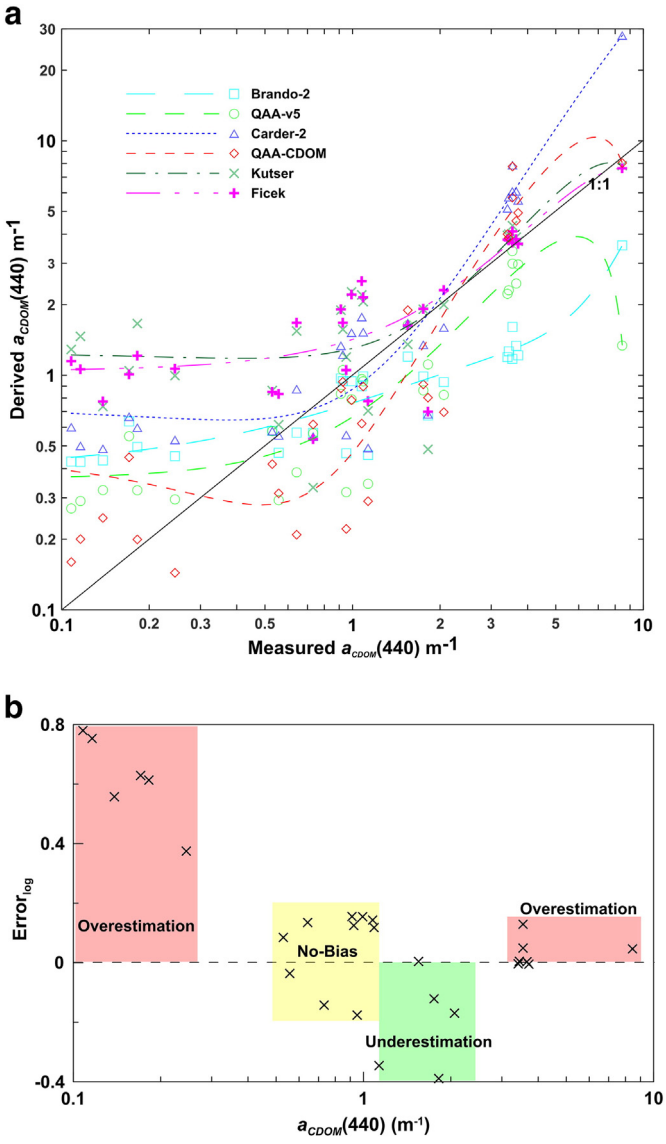

Fig. 6. Assessment of the best six algorithms. (a) Measured vs. derived $a_{CDOM}(440)$. The lines are the trend lines in polynomial fitting the derived data. (b) Errors vs. measured CDOM, where errors were calculated by Eq. (7) and the derived concentration were from the mean of the six algorithms.

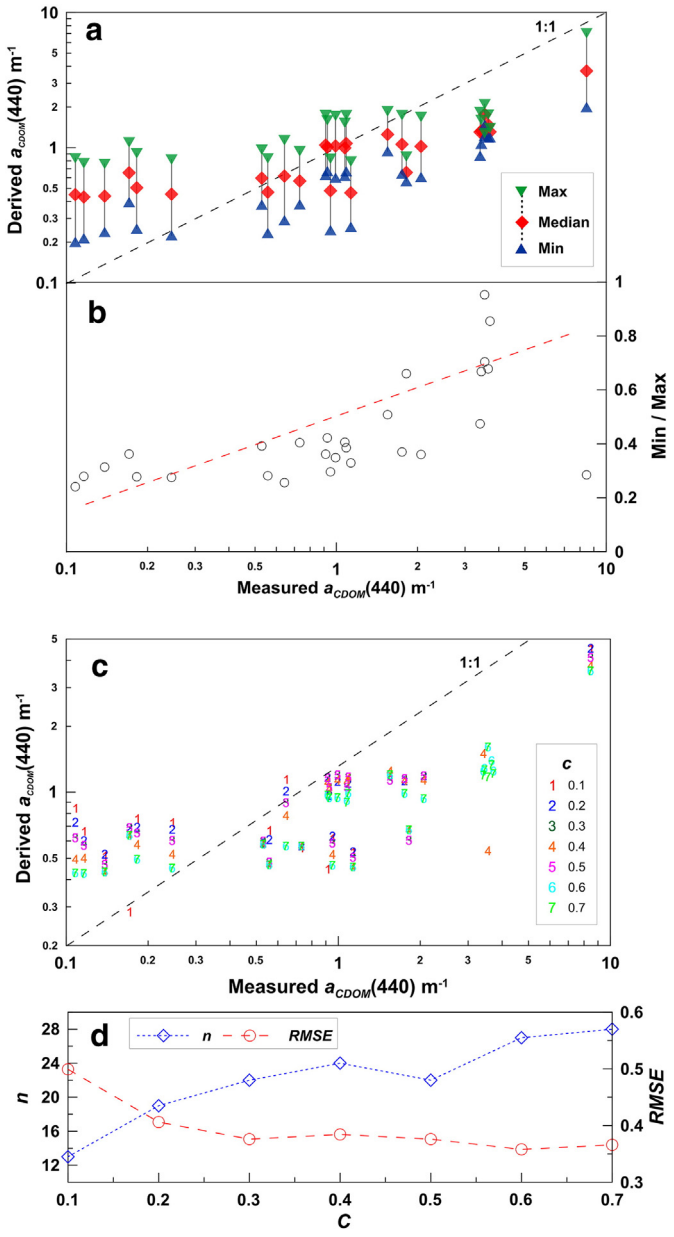

Fig. 7. The effects of SIOPs and criterion *C* on the Brando algorithm. (a) The minimum, median, maximum derived *aCDOM*(440) by setting $0.01 < S < 0.02$ and $0.1 < Y < 0.2$. (b) The min–max ratio vs. the measured *aCDOM*(440). (c) The derived *aCDOM*(440) by using different criteria *C* from 0.1 to 0.7. (d) The number of valid output *n* and RMSE at each given *C*.

in order to effectively set operation parameters. Our results indicate that four parameters influenced MIM output the most: SIOPs (specific inherent optical properties), constant criterion *C*, g_0 and g_1.

3.2.4.1. Effects of SIOPs. SIOPs usually include the specific absorption coefficients of Chl (a_{ph}^*), CDOM slope *S*, and the decay backscattering index *Y*. These optical properties are determined by the physical, chemical and biological properties of the water column, including chlorophyll, CDOM and particles. Two approaches are typically used when implementing MIM algorithms, fixed SIOPs (i.e. Lyon's) or the use of flexible SIOPs (Boss's and Brando's1–2). When flexible slopes are used, MIM algorithms will return a range of $a_{CDOM}(440)$ estimations rather than a single $a_{CDOM}(440)$ as with fixed SIOPs. When a range of $a_{CDOM}(440)$ estimations were generated, we used the median of this range as the value used in evaluation.

In this investigation, we set the flexible SIOPs across a range of $0.01 < S < 0.02$ and the decay backscattering index across a range of $0.1 < Y < 0.2$ as suggested by Boss. The results (Table 3) show that MIM's performances have not been necessarily improved by using flexible instead of fixed SIOPs. The Lyon's results (RMSE 0.61) are even better than the Boss's (RMSE 0.70), but using the same flexible SIOPs, the Brando's results are the best (RMSE 0.36) of the three MIM. Our results also indicated that the use of the median value when flexible SIOPs generated a range of CDOM estimates was only best for medium CDOM waters ($2.0\,m^{-1} > a_{CDOM}(440) > 0.5\,m^{-1}$). For low CDOM waters ($a_{CDOM}(440) < 0.3\ m^{-1}$), the minimum of the range instead of the median resulted in the best calibration (Fig. 7a). For high CDOM waters ($a_{CDOM}(440) > 2.0\,m^{-1}$), the maximum of the range resulted in the best calibration (Fig. 7a). In addition, when CDOM levels were increased, the min–max ratios tended to approach 1 (Fig. 7b), indicating that setting SIOP ranges was more sensitive on low-CDOM than high-CDOM waters.

3.2.4.2. Effects of criterion C. MIM algorithms define a parameter C as a means by which the relationship between measured r_{rs} (remote sensing reflectance just below the water surface) and reconstructed r_{rs} (refer to

Chapter 8 in IOCCG, 2006 for how to reconstruct r_{rs}) is constrained (Eq. (8)).

$$\frac{r_{rs}^{reconstructed} - r_{rs}^{measured}}{r_{rs}^{measured}} < C. \quad (8)$$

When a rigid criterion was chosen (e.g. $C = 0.1$), MIM algorithm output was invalid approximately 50% of the time. This invalid output indicates that no solution could be determined for a given measured r_{rs}. Our results also showed that when C was increased from 0.1 to 0.7, a valid output was achieved for all 28 samples (Fig. 7d). Our investigation indicates that a larger C is more appropriate for complex, CDOM-rich inland waters rather than the small C as reported by Boss as being most effective for clear, CDOM-poor seawater. For example, for CDOM-low water ($a_{CDOM}(440) < 0.3\ m^{-1}$), setting C at a value of 0.6 or 0.7 resulted in the lowest error while $C = 0.1$ resulted in the highest CDOM estimation error (Fig. 7c). Boss and Roesler also suggested that use of wavelengths 410 nm and 670 nm enabled their algorithm to further improve MIM (IOCCG, 2006).

3.2.4.3. Effects of g_0 and g_1. Brando recently reported that MIM algorithms are also sensitive to the a priori parameters g_0 and g_1 used for determining an intermediate variable u, where,

$$u = \frac{-g_0 + \sqrt{g_0^2 + 4g_1 r_{rs}}}{2g_1}. \quad (9)$$

Three different sets of g_0 and g_1 values have been suggested: (1) g_{Gor}: $g_0 = 0.0949$, $g_1 = 0.0794$, suggested by Gordon for Case 1 simple water, (2) g_{Lee}: $g_0 = 0.084$, $g_1 = 0.17$, suggested by Lee for Case 2 complex water, and (3) g_{QAA}: $g_0 = 0.0895$, $g_1 = 0.1247$, for intermediate water used by QAA (Lee et al., 2002). Our results indicate that the substitution of one set for another had no significant effect on MIM algorithm performance. Changing g_0 and g_1 from those suggested by g_{Lee} to g_{Gor} only slightly improved the CDOM estimations in Boss's algorithm ($RMSE\_g_{Lee} = 0.76$ and $RMSE\_g_{Gor} = 0.70$) and had virtually no influence on the Brando algorithm estimation performance ($RMSE\_g_{Lee} = 0.37$ and $RMSE\_g_{Gor} = 0.36$) as shown in Table 3.

While it was indeed true that the g_0 and g_1 values reported in the literature were interchangeable with respect to algorithm output, it was unclear to us if these values were indeed optimal or appropriate for our study area. Thus, we performed a series of algorithm runs in order to conduct a sensitivity analysis of the influence of a wider range of g_0 and g_1 values on algorithm performance. We tested g values across a range of $0.1 < g_0 < 0.2$ and $0.1 < g_1 < 0.3$ with an interval of 0.01 (a total of 600 combinations) for three representative samples (S1, S6, and S9). As one might assume based on the highly varied range of CDOM levels sampled for this study, the best algorithm performance was achieved across a range of g_0 and g_1 pairings, each specific to sample characteristics and SIOPs (Fig. 8).

As the highly varied color patterns in Fig. 8 illustrate, setting optimal g_0 and g_1 values is very data dependent, and they should not be viewed as static analytical parameters. Figs. 8a through 9e illustrate underestimation errors, where the warmer colors represent zones of g_0 and g_1 pairings that resulted in the lowest relative underestimation error. Fig. 8f is unique in that it actually illustrates a zone of little or no error (yellow), while relatively high underestimation and overestimation are represented by the extremes of the color range

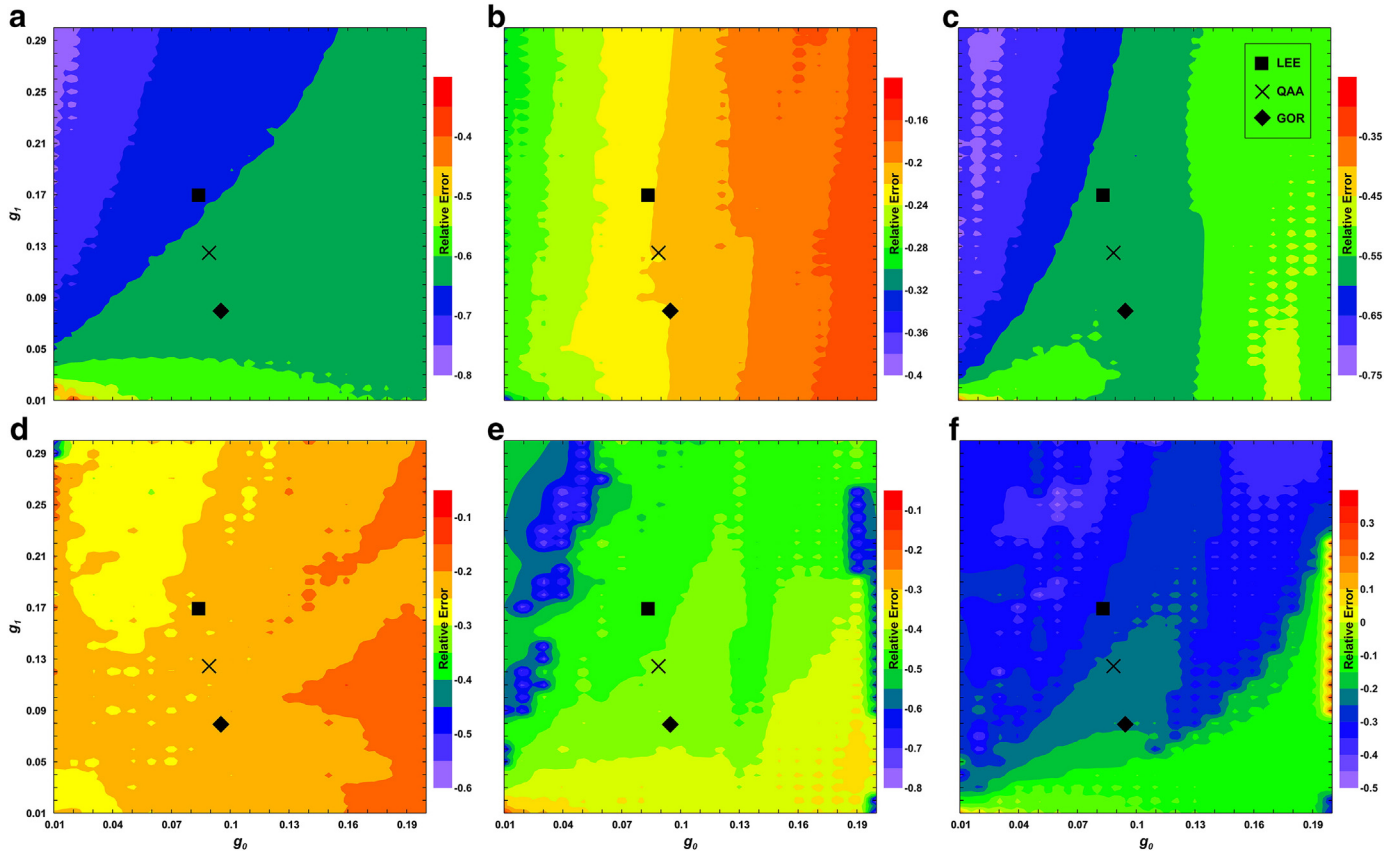

Fig. 8. Maps of relative errors between derived and measured *aCDOM*(440) calculated from 600 combinations of g_0 and g_1, for three samples (S1, S6 and S9), using MIM, 7 bands. (a) S1: S = Median, $C = 5$, $V = 599$, $E = (-0.33, -0.64, -0.79)$, where S, C, and V denote SIOPs, criteria, and valid outputs, and E denotes the minimal, median, and maximal relative errors. (b) S6: S = Median, $C = 5$, $V = 600$, $E = (-0.38, -0.21, -0.15)$ (c) S9: S = Median, $C = 5$, $V = 600$, $E = (-0.75, -0.56, -0.32)$ (d) S6: S = Median, $C = 0.1$, $V = 599$, $E = (-0.61, -0.23, -0.13)$ (e) S9: S = Median, $C = 0.1$, $V = 536$, $E = (-0.79, -0.44, -0.11)$ (f) S9: S = Max, $C = 0.1$, $V = 536$, $E = (-0.50, -0.25, 0.35)$. The three symbols mark the g_0 and g_1 values for three suggestions: GOR, $g_0 = 0.0949$, $g_1 = 0.0794$, QAA, $g_0 = 0.0895$, $g_1 = 0.1247$, and LEE, $g_0 = 0.084$, $g_1 = 0.17$.

shown. For example, given a large criterion $C = 5$, the best g_0 and g_1 for S1 and S9 clusters in a very small region of Fig. 8 where $g_0 \approx g_1 \approx 0.01$ (see red regions in Fig. 8a and c). In contrast, the same region returned the worst results for sample S6 (Fig. 8b), which highlights how it is not possible to select a viable range of g_0 and g_1 values for all applications. The results also indicated that it is best to use a relatively large g_0 (~0.2) in combination with a relatively small g_1 (~0.01) value in MIM algorithms for complex inland water of the study site. It is worth for a further investigation for different freshwater environments. Recently, Brando et al reported that using g_{Lee} is much better than g_{Gor} and g_{QAA} for retrieval $a_{dg}(440)$ for CDOM-rich turbid waters in Fitzroy Estuary and Keppel Bay in Australia.

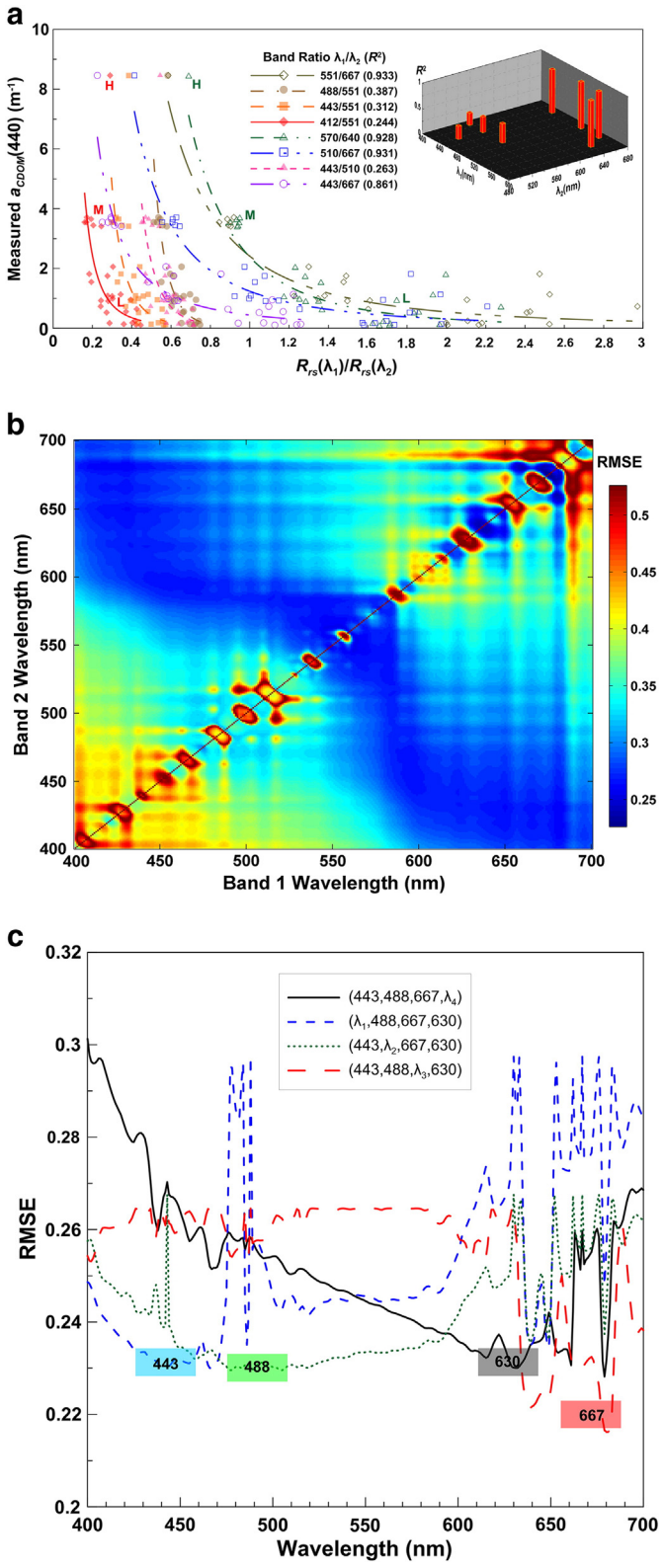

Fig. 9. (a) Correlations between different band ratios and $a_{CDOM}(440)$ (H, M, L are CDOM for high, medium, and low levels, respectively). (b) Estimation error (RMSE) resulting from band ratio optimization for the Fieck, Kutser, and D'Sa models (c) The best 4 bands for the Carder-2 algorithm.

3.2.5. Band effects on algorithm performance

An issue relevant to all remote sensing based CDOM inversion algorithms is the need for quality spectra to be recorded across several wavelengths or bands. This spectral information has the potential to substantially impact the overall performance of the algorithms, some more than others. Three spectral characteristics determine the degree to which the collected spectra influence algorithm output: band/wavelength selection, band ratios and bandwidth (FWHM).

3.2.5.1. Band selection. Our results illustrate that the performance of CDOM algorithms in complex inland waters can be significantly improved by selecting bands with wavelengths longer than those typically selected for ocean environments. For example, the accuracy was improved when 640 nm used in QAA-v4 (RMSE 0.35) was replaced with 667 nm in QAA-v5 algorithm (RMSE 0.31). The Carder-2 algorithm performed far better (RMSE 0.35) than its predecessor Carder-1(RMSE 1.43) when it incorporated a second band at 667 nm. Brando et al (Brando et al., 2012) used two additional bands, 640 and 667 nm, in a MIM algorithm, which yielded a much lower error (RMSE 0.36 vs. 0.75) than the algorithms of D'Sa and Mannino that did not include any bands >600 nm. Our results also indicate that these relatively longer wavelengths (>600 nm) are more appropriate for inland CDOM-rich waters for which the optical properties are heavily influenced by constituents originating from terrestrial vegetation. The utility of these longer wavelength bands is consistent with the results of our previous studies of the Hackensack River, Passaic River, and Newark Bay regions (Yu et al., 2010).

Although reflectance at long-wavelength is typically not sensitive to CDOM levels, evidence shows that the algorithm performance can be improved by using additional longer wavelengths. The additional spectral bands in the red or near infrared are helpful in better accounting for detritus particles. The need for red bands to better quantify CDOM in (rich or not) waters might be explained by the presence of significant amounts of particulate matter. Good CDOM estimation resulted from using longer wavelength is not necessarily conflicting to the theory that spectra in shorter wavelengths are more sensitive to CDOM. UV and short wavelengths are still useful for CDOM estimation in CDOM-rich aquatic environment.

3.2.5.2. Band ratio. Simple band ratios, the division of a single band by another, are commonplace throughout the remote sensing community. One or more simple band ratios serve as the foundation for nonlinear and linear regressions against measured CDOM values to generate coefficients as parameters for empirical algorithms. For example, Carder-1, Carder-2, D'Sa, Kutser and Ficek are all empirical CDOM algorithms that incorporate simple band ratios (See Appendix A).

In order to better understand how the bands selected for a band ratio influenced algorithm performance, we analyzed the influence of band ratio membership on eight common CDOM algorithms. Fig. 9a illustrates that overall CDOM estimation accuracy was low when the simple band ratios were constructed with both bands set at values <550 nm (R^2 = 0.24 – 0.39). In contrast, similar models that incorporated one or more bands that were >560 nm achieved much better predictions (R^2 = 0.861–0.933) for CDOM-rich waters. When including bands of only <560 nm, the resulting band ratios displayed relatively narrow ranges along the x-axis of Fig. 9a (R_{rs}(412/551): 0.15–0.45; R_{rs}(443/551): 0.29–0.57; R_{rs}(488/551): 0.5–0.75; R_{rs}(443/

510): 0.44–0.71). When the range created via a band ratio was compressed, it became increasingly difficult for the model to delineate differences between low, medium and high measured CDOM values, and a poor overall performance is the result. This concept can be visualized by drawing a single vertical line within any band ratio range in Fig. 9a. If one vertical line intercepts low, medium and high measured CDOM values, then this band ratio is not well suited for the optical nature of the sample being evaluated. For example, although CDOM absorption coefficients for the samples in high-CDOM group (H), medium-CDOM (M), and Low-CDOM (L) as shown in Fig. 9a are 8.46, 3.45, and 0.95 m^{-1}, respectively, their band ratios are all approximately 0.39. Therefore it is difficult to distinguish between the varied CDOM levels using the band ratio R_{rs}(443/551). Comparatively, when the models included bands >550 nm, (e.g. 640 nm and 667 nm), the band ratio values were spread across a wider (R_{rs}(570/640): 0.6–2.4; R_{rs}(510/667): 0.3–2.2; R_{rs}(551/667): 0.5–3.0; R_{rs}(443/667): 0.2–1.3). The corresponding CDOM absorption coefficients for the low, medium and high sample groups can be clearly distinguished using the R_{rs}(551/667) band-ratio (low 0.51, medium 0.82, and high 1.39). The inset figure of Fig. 9a also demonstrated that the band-ratio performance by setting at least the second band within 640–670 nm ($R^2 \approx 0.9$) was much better than setting the two bands both at <550 nm ($R^2 \approx 0.3$). These band ratio optimization results strongly suggest that a one or more bands within the red wavelength domain (600–700 nm) is critical for estimation of CDOM via empirical models for CDOM-rich inland waters. Our results were also supported by a recent finding that the best CDOM estimations resulted when both bands were set at >600 nm (Attila et al., 2013). Kallio et al. (2001) also introduced similar results that using green and red/NIR bands improved performance over only using blue and red bands.

The low RMSE region in the lower right corner of Fig. 9b illustrates an area with optimal band ratio selection for the Ficek, Kutser and D'Sa 2-band ratio models. Relative CDOM estimation performance increased (error was reduced) when one band was selected within the range of 400–450 nm and the other band was selected within the range of 630–650 nm. Some CDOM algorithms utilize more than 2 bands within their band ratios. For example, Carder–2 incorporates 4 bands combined to form three band ratios (443/551, 488/551, and 667/551 nm). Note that all of the ratios have the same denominator. We used a band-tuning method (Dall'Olmo & Gitelson, 2006; Gitelson et al., 2008) to determine the best 4 bands in Carder-2. We first evaluated algorithm performance by conducting Carder-2 runs where the denominator was varied from 400 to 700 nm (Fig. 9c) while the numerators were left as their default values (443 nm, 488 nm and 667 nm). The results (Fig. 9c) indicated that the best wavelength domain to be used as the denominator (i.e. lowest RMSE) should be centered at 630 nm. We then used this newly optimized denominator (630 nm) and conducted additional tests in which each of the default numerator values was optimized. Results demonstrated that all three default values are already in their optimized bands.

3.2.5.3. Bandwidth. We also tested whether or not bandwidth had an impact on CDOM estimation accuracy. The Griffin and Kutser algorithms both incorporate wide bands (i.e. Landsat ETM+) rather than the narrow bands used by other CDOM algorithms. Our results (Table 3) show that using narrower bands within these algorithms had no significant influence of algorithm performance. As shown in Table 3, Kutser's algorithm resulted in an overall RMSE_n of 0.45 (n for narrow band) vs. an overall RMSE_w of 0.48 (w for wide band). Similarly, the Griffin's algorithm resulted in an overall RMSE_n of 0.61 vs. an RMSE_w of 0.60. Both display little improvement when narrow bands were used.

Interestingly, Kuster's algorithm did show a significant increase in RMSE (from 0.06 to 0.18) when narrow bands were used for high-CDOM waters. Recall that Kutser's algorithm was developed to incorporate the use of wide bands and was calibrated from high-CDOM waters. Since this algorithm was specifically designed to perform best with wide bands and within CDOM-rich waters, it seems logical that including narrower bands would cause its RMSE specific to high-CDOM waters to increase.

4. Conclusions

CDOM levels in complex freshwaters often display a very broad range influenced by terrestrial characteristics (e.g. vegetation type or quantity) and seasonal differences (i.e. elevated spring soil carbon leachates). CDOM levels in our site vary from 0.11 to 8.46 m^{-1} and have demonstrated a strong correlation with DOC ($R^2 = 0.93$). The complexity of these freshwater environments presents a challenge to current remote sensing algorithms used to estimate biological and chemical water properties. Through evaluating some representative CDOM algorithms via comparisons against in-situ CDOM measurements, this study identified several key observations with respect to the use of current algorithms for estimating the often highly varied CDOM levels in freshwater ecosystems. In general, the algorithms consistently overestimated for low-CDOM waters ($Error_{log}$ >0.4). The consistent underestimation indicated that the tested algorithms need to be improved for the CDOM-poor aquatic environments, e.g., the complex estuarine and lakeshore regions of Lake Huron.

The best six algorithms were QAA-CDOM, QAA-v5, Carder-2, Brando-2, Kutser, and Ficek. Overall estimation performance statistics for all algorithms combined were: RMSE = 0.57, AME = 90%, Bias = −0.71, and $R^2 = 0.58$. These statistics illustrated that the CDOM estimation errors in freshwaters are generally much larger than those generated from scenarios of open-sea waters.

The semi-analytical inversion algorithms (QAA-v4, QAA-v5 and QAA-CDOM) consistently outperformed the others across all water scenarios (low, medium and especially high CDOM level waters). Our results show that QAA-CDOM is indeed optimized for a broader range of CDOM absorptivity, and represents a significant improvement over its predecessors. Comparative analysis confirmed that using separate absorption coefficients for complex freshwater as with the QAA-CDOM algorithm is advantageous because it reduces the interference from high concentrations of sediments and chl-a in freshwater environments.

The empirical algorithms (Carder-1, Carder-2, Mannino, D'Sa, Griffin, Del Castillo Kutser and Ficek) when developed with large data sets spanning broad environmental conditions performed well where $a_{CDOM}(440) < 1\ m^{-1}$. Empirical algorithms often include reflectance from two or more bands structured in one or more band ratios as evident in Appendix A. Our results illustrate that the performance of empirical algorithms in complex inland waters can be significantly improved by selecting at least one band with a relatively longer wavelength (>600 nm), especially when the water optical properties are heavily influenced by constituents originating from terrestrial vegetation. Since chlorophyll and non-algal particles are usually in high concentrations and also present high back-scattering within the longer wavelengths, the results suggest usefulness of using these longer wavelengths for CDOM estimation by reducing the possible effects of particulate matter. Our outcome might spawn further research into the botanical basis of this link between terrestrial (vs. aquatic) vegetation and these longer wavelengths with CDOM models. Carder-2 is representative of empirical models that incorporate 4 or more bands structured in predefined band ratios with static numerators and denominators. We found that substituting a second band with a longer wavelength >600 nm as the denominator substantially improved the performance of band-ratio-based algorithms. The default numerator wavelengths of 443, 448 and 667 nm were determined to be applicable to complex freshwater environments.

Fixed or flexible SIOPs can be used with little effect on MIM (Lyon, Boss and Brando) algorithm performance. In those instances where flexible SIOPs are used, the median value is most appropriate for medium-CDOM waters, the minimum for low-CDOM waters and the maximum for high-CDOM waters. In addition, our analysis indicates that a larger C is more appropriate for MIM algorithms when applied to complex, CDOM-rich inland waters as opposed to the small C that has proven effective for clear, CDOM-poor seawater. Well established g_0 and g_1 MIM algorithm parameters can be substituted with little or no effect on estimation performance. It should be noted that these values were found to be less than optimal within our study site due to its highly varied CDOM levels. Ultimately, the best MIM algorithm performance was achieved across a varied range of g_0 and g_1 pairings, each specific to sample characteristics and SIOPs. Generally, our results indicate that it is best to utilize a relatively large g_0 (~0.2) in combination with a relatively small g_1 (~0.01) value for the MIM algorithms when applied to complex freshwater environments.

We also would like to emphasize that our algorithm assessment was based on just above-surface measurements using HyperSAS. Algorithm performance will be generally worsened when using satellite sensors because of many uncertainty factors, such as the atmospheric effects, sensor signal-to-noise ratio and viewing geometry. The evaluation results from using satellite images are not included in this manuscript which is to focus on algorithm evaluation instead of sensor evaluation.

Acknowledgment

This research is partially supported by an internal grant from Central Michigan University and two collaborative grants from the National Science Foundation (Grant #: 1025547; Grant #: 1230261). We thank Dr. Uzarski D.G., Dr. Kevin H. Wyatt and Mr. Thomas Clement for measuring the DOC concentrations and Dr. Learman D.R. for sharing the spectrophotometer in his laboratory for measuring the CDOM absorption coefficients. All authors appreciate the many constructive suggestions and valuable comments from anonymous reviewers.

Appendix A

Formulas of empirical CDOM retrieval algorithms,

Carder-1

$$a_{dg}(443) = 10^{\left(-1.144-0.738p_{15}-1.386p_{15}^2-0.644p_{25}+2.451p_{25}^2\right)} \quad \text{(A1)}$$

where $p_{15} = R_{rs}(412)/R_{rs}(551)$, $p_{25} = R_{rs}(443)/R_{rs}(551)$.
Carder-2

$$a_{dg}(443) = 10^{(0.043-0.185p_{25}-1.081p_{35}+1.234p_{65})} \quad \text{(A2)}$$

where $p_{25} = R_{rs}(443)/R_{rs}(551)$, $p_{35} = R_{rs}(488)/R_{rs}(551)$, $p_{65} = R_{rs}(667)/R_{rs}(551)$.
Ficek:

$$a_{CDOM}(440) = 3.65\left(\frac{R_{rs}(570)}{R_{rs}(655)}\right)^{-1.93}. \quad \text{(A3)}$$

Mannino

$$a_{CDOM}(443) = -0.0736ln\left(\frac{0.408R_{rs}(490)}{R_{rs}(555)} - 0.173\right). \quad \text{(A4)}$$

Griffin

$$a_{CDOM}(400) = \exp\left(-1.145 + 26.529\mathrm{TM}_3 + 0.603\frac{\mathrm{TM}_2}{\mathrm{TM}_1}\right) \quad \text{(A5)}$$

where TM1–TM3 are atmospherically corrected reflectance of Landsat TM or ETM + band 1 (450–520 nm), band 2 (520–600 nm) and band 3 (630–690 nm).
Del Castillo

$$a_{CDOM}(412) = -0.90\left(\frac{R_{rs}(510)}{R_{rs}(670)}\right) + 2.34. \quad \text{(A6)}$$

D'Sa

$$a_{CDOM}(412) = 0.134\left(\frac{R_{rs}(443)}{R_{rs}(510)}\right)^{-2.025}. \quad \text{(A7)}$$

Kutser

$$a_{CDOM}(420) = 5.13\left(\frac{\mathrm{B2}}{\mathrm{B3}}\right)^{-2.67} \quad \text{(A8)}$$

where B2 and B3 are from atmospherically corrected ALI images, that is, irradiance reflectance $R(525–605)$ and $R(630–690)$.

References

Ammenberg, P., Flink, P., Lindell, T., Pierson, D., & Strombeck, N. (2002). Bio-optical modelling combined with remote sensing to assess water quality. *International Journal of Remote Sensing*, *23*, 1621–1638.
Attila, J., Koponen, S., Kallio, K., Lindfors, A., Kaitala, S., & Ylostalo, P. (2013). MERIS case II water processor comparison on coastal sites of the northern Baltic Sea. *Remote Sensing of Environment*, *128*, 138–149.
Blough, N. V., & Vecchio, R. D. (2001). *Chromophoric DOM in the coastal environment.* Biogeochemistry of marine dissolved organic matter. San Diego Academic Press, 509–546.
Blough, N. V., Zafiriou, O. C., & Bonilla, J. (1993). Optical-absorption spectra of waters from the Orinoco River outflow — terrestrial input of colored organic-matter to the Caribbean. *Journal of Geophysical Research-Oceans*, *98*, 2271–2278.
Bowers, D.G., & Brett, H. L. (2008). The relationship between CDOM and salinity in estuaries: An analytical and graphical solution. *Journal of Marine Systems*, *73*, 1–7.
Bracchini, L., Dattilo, A.M., Hull, V., Loiselle, S. A., Martini, S., Rossi, C., et al. (2006). The bio-optical properties of CDOM as descriptor of lake stratification. *Journal of Photochemistry and Photobiology. B, Biology*, *85*, 145–149.
Brando, V. E., & Dekker, A. G. (2003). Satellite hyperspectral remote senseing for estimating estuarine and coastal water quality. *IEEE Transactions on Geoscience and Remote Sensing*, *41*, 1378–1387.
Brando, V. E., Dekker, A. G., Park, Y. J., & Schroeder, T. (2012). Adaptive semianalytical inversion of ocean color radiometry in optically complex waters. *Applied Optics*, *51*, 2808–2833.
Brezonik, P., Menken, K. D., & Bauer, M. (2005). Landsat-based remote sensing of lake water quality characteristics, including chlorophyll and colored dissolved organic matter (CDOM). *Lake and Reservoir Management*, *21*, 373–382.
Carder, K. L., Chen, F. R., Lee, Z. P., Hawes, S. K., & Kamykowski, D. (1999). Semianalytic moderate-resolution imaging spectrometer algorithms for chlorophyll a and absorption with bio-optical domains based on nitrate-depletion temperatures. *Journal of Geophysical Research-Oceans*, *104*, 5403–5421.
Chen, R. F., Bissett, P., Coble, P., Conmy, R., Gardner, G. B., Moran, M.A., et al. (2004). Chromophoric dissolved organic matter (CDOM) source characterization in the Louisiana Bight. *Marine Chemistry*, *89*, 257–272.
Dall'Olmo, G., & Gitelson, A. A. (2006). Effect of bio-optical parameter variability and uncertainties in reflectance measurements on the remote estimation of chlorophyll-a concentration in turbid productive waters: Modeling results. *Applied Optics*, *45*, 3577–3592.
Del Castillo, C. E., Coble, P. G., Morell, J. M., Lopez, J. M., & Corredor, J. E. (1999). Analysis of the optical properties of the Orinoco River plume by absorption and fluorescence spectroscopy. *Marine Chemistry*, *66*, 35–51.
Del Castillo, C. E., & Miller, R. L. (2008). On the use of ocean color remote sensing to measure the transport of dissolved organic carbon by the Mississippi River plume. *Remote Sensing of Environment*, *112*, 836–844.
D'Sa, E. J., & Miller, R. L. (2003). Bio-optical properties in waters influenced by the Mississippi River during low flow conditions. *Remote Sensing of Environment*, *84*, 538–549.
Ficek, D., Zapadka, T., & Dera, J. (2011). Remote sensing reflectance of Pomeranian lakes and the Baltic. *Oceanologia*, *53*, 959–970.
Gitelson, A. A., Dall'Olmo, G., Moses, W., Rundquist, D. C., Barrow, T., Fisher, T. R., et al. (2008). A simple semi-analytical model for remote estimation of chlorophyll-a in turbid waters: Validation. *Remote Sensing of Environment*, *112*, 3582–3593.
Griffin, C. G., Frey, K. E., Rogan, J., & Holmes, R. M. (2011). Spatial and interannual variability of dissolved organic matter in the Kolyma River, East Siberia, observed using satellite imagery. *Journal of Geophysical Research-Biogeosciences*, *116*, 12.
Hoge, F. E., & Lyon, P. E. (1996). Satellite retrieval of inherent optical properties by linear matrix inversion of oceanic radiance models: An analysis of model and radiance measurement errors. *Journal of Geophysical Research-Oceans*, *101*, 16631–16648.

Hoge, F. E., & Lyon, P. E. (2002). Satellite observation of chromophoric dissolved organic matter (CDOM) variability in the wake of hurricanes and typhoons. *Geophysical Research Letters*, *29*.

Hoge, F. E., Wright, C. W., Lyon, P. E., Swift, R. N., & Yungel, J. K. (1999). Satellite retrieval of inherent optical properties by inversion of an oceanic radiance model: A preliminary algorithm. *Applied Optics*, *38*, 495–504.

Hoge, F. E., Wright, C. W., Lyon, P. E., Swift, R. N., & Yungel, J. K. (2001). Inherent optical properties imagery of the western North Atlantic Ocean: Horizontal spatial variability of the upper mixed layer. *Journal of Geophysical Research-Oceans*, *106*, 31129–31140.

Hu, C. M., Muller-Karger, F. E., Taylor, C., Carder, K. L., Kelble, C., Johns, E., et al. (2005). Red tide detection and tracing using MODIS fluorescence data: A regional example in SW Florida coastal waters. *Remote Sensing of Environment*, *97*, 311–321.

Huang, W., & Chen, R. F. (2009). Sources and transformations of chromophoric dissolved organic matter in the Neponset River watershed. *Journal of Geophysical Research-Biogeosciences*, *114*, 14.

IOCCG (2000). In S. Sathyendranath (Ed.), *Remote sensing of ocean color in coastal, and other optically-complex, waters*.

IOCCG (2006). In Z. P. Lee (Ed.), *Remote sensing of inherent optical properties: fundamentals, tests of algorithms, and applications*.

Kallio, K., Kutser, T., Hannonen, T., Koponen, S., Pulliainen, J., Vepsalainen, J., et al. (2001). Retrieval of water quality from airborne imaging spectrometry of various lake types in different seasons. *Science of the Total Environment*, *268*, 59–77.

Kutser, T., Pierson, D. C., Kallio, K. Y., Reinart, A., & Sobek, S. (2005). Mapping lake CDOM by satellite remote sensing. *Remote Sensing of Environment*, *94*, 535–540.

Kutser, T., Pierson, D., Tranvik, L., Reinart, A., Sobek, S., & Kallio, K. (2005). Using satellite remote sensing to estimate the colored dissolved organic matter absorption coefficient in lakes. *Ecosystems*, *8*, 709–720.

Lee, Z. P., Carder, K. L., & Arnone, R. A. (2002). Deriving inherent optical properties from water color: A multiband quasi-analytical algorithm for optically deep waters. *Applied Optics*, *41*, 5755–5772.

Lee, Z. P., Lubac, B., Werdell, J., & Arnone, R. (2009). An update of the quasi-analytical algorithm (QAA_v5). http://www.ioccg.org/groups/Software_OCA/QAA_v5.pdf

Lee, Z. P., Weidemann, A., Kindle, J., Arnone, R., Carder, K. L., & Davis, C. (2007). Euphotic zone depth: Its derivation and implication to ocean-color remote sensing. *Journal of Geophysical Research-Oceans*, *112*.

Liu, C. C., & Miller, R. L. (2008). Spectrum matching method for estimating the chlorophyll-a concentration, CDOM ratio, and backscatter fraction from remote sensing of ocean color. *Canadian Journal of Remote Sensing*, *34*, 343–355.

Mannino, A., Russ, M. E., & Hooker, S. B. (2008). Algorithm development and validation for satellite-derived distributions of DOC and CDOM in the US Middle Atlantic Bight. *Journal of Geophysical Research-Oceans*, *113*, 19.

Maritorena, S., Siegel, D. A., & Peterson, A.R. (2002). Optimization of a semianalytical ocean color model for global-scale applications. *Applied Optics*, *41*, 2705–2714.

Matthews, M. W. (2011). A current review of empirical procedures of remote sensing in inland and near-coastal transitional waters. *International Journal of Remote Sensing*, *32*, 6855–6899.

Miller, R. L., Del Castillo, C. E., & Mckee, B.A. (2005). *Remote sensing of coastal aquatic environments: Technologies, techniques, and applications.* Springer.

Mobley, C. D. (1999). Estimation of the remote-sensing reflectance from above-surface measurements. *Applied Optics*, *38*, 7442–7455.

Nelson, N.B., & Siegel, D. A. (2002). Chromophoric DOM in the open ocean. In A.D. Hansell, & A.C. Carlson (Eds.), *Biochemistry of marine dissolved organic matter*. San Diego Academic Press.

Sandidge, J. C., & Holyer, R. J. (1998). Coastal bathymetry from hyperspectral observations of water radiance. *Remote Sensing of Environment*, *65*, 341–352.

Sathyendranath, S., & Platt, T. (1997). Analytic model of ocean color. *Applied Optics*, *36*, 2620–2629.

Stedmon, C. A., Markager, S., Sondergaard, M., Vang, T., Laubel, A., Borch, N. H., et al. (2006). Dissolved organic matter (DOM) export to a temperate estuary: Seasonal variations and implications of land use. *Estuaries and Coasts*, *29*, 388–400.

Tanaka, A., & Oishi, T. (1998). Application of the neural network to OCTS data. In S. Ackleson (Ed.), *Proceedings, ocean optics, XIV*, Washington DC Office of Naval Research.

Vlahos, P., Chen, R. F., & Repeta, D. J. (2002). Dissolved organic carbon in the Mid-Atlantic Bight. *Deep-Sea Research Part II-Topical Studies in Oceanography*, *49*, 4369–4385.

Wang, P., Boss, E. S., & Roesler, C. (2005). Uncertainties of inherent optical properties obtained from semianalytical inversions of ocean color. *Applied Optics*, *44*, 4074–4085.

Yu, Q., Tian, Y. Q., Chen, R. F., Liu, A., Gardner, G. B., & Zhu, W. N. (2010). Functional linear analysis of in situ hyperspectral data for assessing CDOM in rivers. *Photogrammetric Engineering and Remote Sensing*, *76*, 1147–1158.

Zhu, W. N. (2011). Inversion and analysis of chromophoric dissolved organic matter in estuarine and coastal regions using hyperspectral remote sensing. *Department of Geosciences*. Amherst, MA University of Massachusetts Amherst.

Zhu, W. N., Tian, Y. Q., Yu, Q., & Becker, B.L. (2013). Using Hyperion imagery to monitor the spatial and temporal distribution of colored dissolved organic matter in estuarine and coastal regions. *Remote Sensing of Environment*, *134*, 342–354.

Zhu, W. N., & Yu, Q. (2013). Inversion of chromophoric dissolved organic matter (CDOM) from EO-1 Hyperion imagery for turbid estuarine and coastal waters. *IEEE Transactions on Geoscience & Remote Sensing*, *51*, 3286–3298.

Zhu, W. N., Yu, Q., & Tian, Y. Q. (2013). Uncertainty analysis of remote sensing of colored dissolved organic matter: Evaluations and comparisons for three rivers in North America. *ISPRS Journal of Photogrammetry and Remote Sensing*, *84*, 12–22.

Zhu, W. N., Yu, Q., Tian, Y. Q., Chen, R. F., & Gardner, G. B. (2011). Estimation of chromophoric dissolved organic matter in the Mississippi and Atchafalaya river plume regions using above-surface hyperspectral remote sensing. *Journal of Geophysical Research-Oceans*, *116*, C02011.